Variability of kinematic source parameters and its implication on the choice of the design scenario

Giovanna Cultrera, Antonella Cirella, Elena Spagnuolo, André Herrero, Elisa Tinti, Francesca Pacor

Istituto Nazionale di Geofisica e Vulcanologia, Italy

Abstract

Near-fault seismic recordings for recent earthquakes (Chi Chi earthquake, 1999; Parkfield earthquake, 2004) show the high spatial heterogeneity of ground motion. This variability is controlled by fault geometry, rupture complexity, and also by wave propagation and site effects. Nowadays, the number of available records in near-source region is still not enough to infer a robust parameterization of the ground motion and to retrieve multi-parametric predictive equations valid at close distances from the fault. The use of a synthetic approach may help to overcome this limitation and to study the strong ground motion variability. In this paper we focus on ground-motion dependence on different earthquakes breaking the same fault, as it has been rarely recorded by instruments. We model seismic scenarios from different rupture models of a fault similar to the 1980 Irpinia, Italy, earthquake source (Mw 6.9). A discrete wavenumber-finite element technique is used to compute full-wave displacement and velocity time series in the low-frequency band (up to 2 Hz).

We investigate the variability of the ground motion as a function of different source parameters (rupture velocity, slip distribution, nucleation point, source time function), whose values depend on the state of knowledge of the physical model driving the process. The probability density functions of the simulated ground motion parameters, such as displacement response spectrum (SD) and peak ground velocity (PGV), have been used to identify particular scenarios that match specific engineering requests.

Introduction

The ground motion due to a seismic event is variable in space and time. The spatial variability at different sites during a single earthquake (*intra*-event variability) depends not only on the heterogeneities of the propagation medium and on the local site conditions, but also on the source effects, like directivity or radiation pattern. Ground motion variation observed at the same site for different earthquakes (*inter*-event variability) is also related to the variation in source characteristics and to the source-to-site geometry.

As a first approximation it is possible to classify two main sources of ground motion variability at bedrock sites: the heterogeneity of propagation medium and the characteristics of the rupture process. However, it is far from simple to unambiguously distinguish the relative influence of these two factors. At large distances from the seismic source (more than 2-3 fault lengths), the variability of the motion at high frequencies is expected to be mainly controlled by the properties of the propagation medium. For instance, Spudich and Chiou (2006) demonstrate that the radiation pattern imprint in this frequency-distance domain tends to vanish. However, the recordings during recent earthquakes (e.g. Chi Chi, 1999; Parkfield 2004) show that the large spatial variability of the ground motion in near-source is mostly due to the fault geometry and to the local variation of the rupture process (e.g. Ma et al., 2000; Shakal et al., 2005).

Unfortunately, only few earthquakes have ruptured the same seismogenic fault more than once in recent times such that recordings could be obtained in the near-source region with high-quality networks (e.g., 1966 and 2004 Parkfield earthquakes, see Harris and Arrowsmith, 2006; 2004 and 2007 Nigata earthquakes, see Cirella et al., 2008). The lack of such observations limits the detailed analysis of the dependence of ground motion on source parameters.

For the time being, the use of synthetic ground motions obtained by realistic simulation approaches may partially overcome the paucity of near-source data (Andrews et al., 2007). The ground motion simulations allow us to assess how the input parameters (source and propagation medium) affect the computed motion in order to clearly separate the causes of the ground motion variability. Moreover, a simulation based approach provides a means to define possible hierarchy among the source parameters in terms of their effect on intensity measures (e.g. Baker and Cornell, 2006).

The use of numerical computation may be limited by several problems. The main one is due to the difficulty of modeling the heterogeneity of source process and Earth structure at all the length scales and, in general, to account for the whole complexity of the involved physical processes. Another

important problem is the limited knowledge of the values of rupture parameters required to model the rupture process (e.g. Bommer and Abrahamson, 2006).

However, recent studies have been focused on the simulations of ground motion for future earthquakes with the purpose of quantifying the variability of source and propagation parameters (e.g., Ameri et al., 2007; Rodgers et al., 2007; Sekiguchi, 2007; Sørensen et al, 2007; Ameri et al., 2008; Causse et al., 2008; Ripperger et al., 2008; Wang et al., 2008). The large amount of synthetic seismograms gives a very detailed description of the variability that could be observed at several sites for different earthquakes. They are used for engineering seismology applications, such as the seismic design of structures and the calculation of Probabilistic Seismic Hazard (PSHA) curves, where the simulated ground motion parameters substitute the predictions from empirical models (Convertito and Herrero, 2004; Convertito et al., 2006; SCEC/CME CyberShake Project, 2007).

Shaking scenarios for engineering applications are generally provided in terms of Peak Ground Acceleration (PGA), Peak Ground Velocity (PGV), Peak Ground Displacement (PGD) and response spectral ordinates (hereafter referred as ground motion parameters or intensity measures) expected at a selected site. Each ground motion parameter represents different characteristics of the seismogram, and is sensitive to a different frequency content in seismic radiation spectrum: the PGD is related to the low frequency motion ($f < 1Hz$) and mainly correlated to the magnitude and focal mechanism, the PGV is controlled by the coherent low-to-intermediate frequency of ground motion (indicatively 1 – 3 Hz) and by the corner frequency, whereas the peak ground acceleration (PGA) depends on the high frequencies which are strongly affected by small scale heterogeneities of rupture and propagation medium. For this reason, different intensity measures are required for engineering applications, depending on the characteristic earthquake (fault and magnitude) in the region of interest, on the type of structures (e.g., buildings, lifelines, infrastructures) and on the particular seismic design under consideration. For example, earthquake resistant design for a long span bridge needs very long-period spectral displacement, whereas for buildings or tunnels the seismic response mostly depends on the high-frequency motion.

For structures having a long vibration period, the seismic action may be represented in the form of a displacement response spectrum (CEN 2004, ANNEX A of EC8-part 1). The same long-period response spectral ordinates are required for displacement-based design approaches and for base isolation devices (Akkar and Bommer, 2007).

The aim of this study is the analysis of the variability of ground motion due to the variation of several kinematic parameters describing the seismic source, through the massive use of synthetic scenario computations. We do not include any variability in ground motions due to variations in site response (the simulations are computed at bedrock sites considering only one propagation model),

being the study of the propagation medium effects and local site conditions beyond the aim of this paper. The analysis allows us to quantify the effect of the rupture process parameters at different stations on several intensity measures. Moreover, we show a possible use of the statistical distributions of synthetic ground motion parameters to select shaking scenarios whose characteristics follow defined criteria, such as scenarios having a particular peak value at one or more sites.

Variability of kinematic parameters

The range of variability of the kinematic parameters describing the fault rupture is generally constrained by scaling laws derived from observations or physically defined by studies on source dynamics. The definition of their values is extremely important for the modeling of ground motion scenarios, because it allows us to limit the number of physically realistic simulations. The variability of a few kinematic source parameters is well known or has been deeply studied in the recent literature, such as for the source time function (STF), the position of nucleation point (NP), the rupture velocity (Vr) and the slip distribution (SLIP) on the fault plane (Aki and Richards, 2002). However, there are other kinematic parameters whose values are still not well constrained. This is the case of the rise time, whose variability has not been investigated in this study.
In this section we summarize the expected ranges and the reference values of the aforementioned four kinematic source parameters that have been varied to build the synthetic scenarios of this work.

Position of the nucleation point (NP)

The location of the nucleation point on the fault plane controls the directivity effect by changing the relative source-to-receiver position. This parameter has large variability: hypocenters are found either in the deeper half-width of the fault but also close to the fault top (Somerville et al., 1999; Manighetti et al., 2005), and a large percentage of them are located either within or close to regions of large slip (Mai et al., 2005). Moreover, repeating fault ruptures can nucleate in different positions, as for the two similar Parkfield earthquakes of 1966 and 2004 that ruptured the same fault plane but with different slip distribution and nucleation position (Custódio and Archuleta, 2007).

Rupture velocity (Vr)

The velocity of the propagating rupture front affects the signal duration and contributes to the directivity effect, which increases as the rupture velocity increases. Moreover, its local variation generates high-frequency radiation.

The description of this parameter is generally simplified, and hence is often assumed constant on the fault plane. However, kinematic rupture histories with variable rupture velocity on the fault have been recently retrieved from non-linear kinematic inversion (e.g., Delouis et al., 2002; Liu and Archuleta, 2004; Piatanesi et al. 2007; Cirella et al., 2008). This behavior is also found in the spontaneous dynamic models, where the variability of the rupture velocity depends on the heterogeneous distribution of dynamic parameters on the fault plane. For example, Ruiz (2007) obtains a rupture velocity proportional to the 4^{th} power of the slip gradient through spontaneous dynamic simulations. For both constant and heterogeneous rupture models, the rupture velocity is defined in general as a fraction of the shear-wave velocity (Vs), ranging between 0.6·Vs and 0.92·Vs (the latter corresponds to the Rayleigh waves velocity). This range is constrained by spontaneous dynamic simulations (Andrews, 1976; Bouchon et al., 2001; Bizzarri et al., 2001 and references therein). The dynamic models predict also rupture velocities greater than the shear velocity under particular values of the constitutive parameters (Andrews, 1976; Rosakis et al., 1999 among many others): in all these models, very high peaks of slip velocity are found and they are believed to be responsible of anomalous wave amplitudes (Bizzarri and Spudich, 2008), as confirmed by kinematic models of recent earthquakes (e.g., 1999 Izmit earthquake in Bouchon et al., 2002; 1999 Duzce earthquake in Birgören et al., 2004; 2002 Denali earthquake in Oglesby et al., 2004).

Slip distribution on the fault (SLIP)

The slip distribution of essentially all earthquakes, imaged by kinematic inversion techniques, is heterogeneous on the fault plane. This heterogeneity can be observed at all scales and it has been modeled by different authors (Hanks, 1979; Andrews, 1980; Frankell, 1991; Zeng et al., 1994; Ma et al., 2000; Shakal et al., 2005). In particular, Herrero and Bernard (1994) proposed a simple method to account for the details of slip in a large range of wavelengths, by using the self similar slip distribution (k^{-2}) on the fault plane.

The heterogeneity often results in different-sized slip patches, whose relative positions with respect to the hypocenter location affect the near-source ground motion and control directivity effects (e.g., Manighetti et al., 2001; Mai et al., 2005).

Source time function (STF)

In a first approximation, the rupture behavior can be described as a simple phenomenon: each point on the fault plane starts to slide when the rupture front reaches its position; the final slip at each point on the fault plane is reached in a specific time interval (called rise time) and its evolution is described through a slip velocity function varying on the fault.

Several authors have proposed different analytical models to parameterize the slip velocity function, on the basis of dynamic rupture modeling: crack-like models (Andrews 1976; Das and Aki, 1977; Day, 1982) and pulse-like models (Heaton 1990; Nielsen and Madariaga, 2003). In the crack-like models the healing is due to the rupture front back-propagating from the fault boundaries; in this case the maximum rise time is comparable to the rupture duration and it depends on the dimension of the fault. In the pulse-like models the rupture front is followed by a healing front and the rise time is shorter and independent from the rupture duration; these models are used in kinematic simulations, the rise time being assumed either variable (e.g. Bernard et al.,1996; Cirella et al. 2008) or constant on the fault (e.g., Beroza and Spudich, 1988; Somerville, 1999). We underline that a realistic characterization of the slip-velocity function is a critical component of earthquake-rupture modeling (Guatteri et al., 2004; Tinti et al., 2009) Moreover, waveform-inversion procedures cannot well invert and resolve the rise time values both because of the limited frequency band considered during the inversion and because of an evident trade-off between rise time and the peak slip velocity.

The functional form of the slip velocity is defined by the source time function (STF). In the single-time window approaches (Cohee and Beroza; 1994), the temporal evolution of slip velocity is described by an analytical expression of STF, usually defined as a boxcar, an exponential, a cosine or a triangle. In this work we also consider a new source time function recently proposed in literature, the regularized Yoffe function (Tinti et al., 2005; Cirella et al., 2006). This is a flexible STF defined by three independent parameters: the final slip, the slip duration and the duration of the positive slip acceleration T_{acc}. This new source time function is consistent with dynamic 'pulse-like' earthquake rupture and it allows the dynamic interpretation of the kinematic slip models (Nielsen and Madariaga, 2003; Piatanesi et al., 2004).

Strategy for ground motion scenarios

In this study we focus on two ground motion parameters, displacement response spectrum (SD) and peak ground velocity (PGV). The first parameter is commonly used for displacement-based design approaches (CEN 2004, ANNEX A of EC8-part 1; Akkar and Bommer, 2007). The second

parameter, PGV, is used in specifying input to engineering design, such as the estimate of macroseismic intensity and structural damage. It is also employed in some methods for the assessment of liquefaction potential and, because of its relationship to ground strains, in the seismic design and assessment of buried pipelines (Bommer and Alacon, 2006; Bommer et al., 2009).

Among the simulation methods proposed in the literature, we use a discrete wave-number/finite element technique (COMPSYN code; Spudich and Xu, 2003); it computes full-wave displacement and velocity time series in the zero-to-intermediate frequency band on an extended fault, allowing us to vary the kinematic source parameters of interest. This technique does not account for the wave attenuation of the Earth. However, in this case study the attenuation effect is negligible because we are considering low-frequency motion at close distances from the fault.

First, we define a fixed fault geometry and different rupture models, obtained by varying the kinematic source parameters, and then compute synthetic displacement and velocity seismograms at several sites. The entire set of synthetic scenarios is then analyzed with the aim to investigate the influence of the variability of kinematic parameters on the ground motion parameters of engineering interest. Moreover, the synthetic data-set can be also used to identify the seismograms whose intensity measures match specific engineering requirements and/or to introduce a statistical analysis of the inferred peak ground motion distributions. The latter can be used to provide a sub-set of scenarios satisfying a particular statistical request (e.g., modal value, maximum probability of occurrence, extreme or mean values, percentiles) or as input in the PSHA formulation (Convertito et al., 2006).

Geometrical setting and fault parameters

We model all scenarios for a single fault plane with a focal mechanism similar to the 1980 Irpinia, Italy, earthquake (Mw 6.9): normal fault of (35x15) km^2, 60° dip, 315° strike, -90° rake, and fault top depth at 2.2 km. The kinematic parameters are assigned at nodal points of the fault plane equally spaced every 100 m along strike and dip directions.

The main goal of this paper is to study the ground motion variability due to the variations of kinematic rupture parameters. We therefore assume a simplified 1-D crustal model valid for the area to compute the Green's functions (Table 1; Amato and Selvaggi, 1993; Improta et al., 2003; Improta, 2009, personal communication) and we do not include any variability in ground motions due to variations in site response.

Synthetic seismograms are computed at bedrock in the frequency band 0-2.0 Hz, for 31 virtual sites and for 12 sites having the same location of the Accelerometric Italian Network stations (ITACA Working Group, 2008; Figure 1). For all sites, the fault distance R_{JB} (defined as the closest distance

to the surface projection of the fault plane; Joyner and Boore, 1981) ranges between 7 km and 70 km.

The different rupture models are obtained by varying the position of the nucleation point, the rupture velocity, the source time function and the final slip distribution. For all cases the rise time is chosen to be constant on the fault and equal to 1 sec. We consider 7 nucleation points (NP) in the deeper portion of the fault, equally spaced along the fault length to account for the potential directive and anti-directive effects (Figure 1). Three distributions of final slip on the fault plane (SLIP model *A*, model *B*, model *C;* Figure 2) are considered; they are computed using a self similar k-square slip model (Herrero and Bernard, 1994). We assume 4 analytical source time functions (STF) describing the slip velocity evolution (Figure 3): a boxcar, an exponential, a cosine and a regularized Yoffe function (Tinti et al., 2005; Cirella et al., 2006) with constant T_{acc}=0.225s. Finally, we consider 3 constant rupture velocities (V_r1, V_r2, V_r3), defined as 70%, 80% (Figure 2d) and 90% of S-wave velocity (V_s= 3.0km/s), and 2 heterogeneous distributions of rupture velocity whose variations depend either on the distance (*dis*) of the rupture front from the nucleation point (V_r4) or on the final slip distribution *D(x,y)* on the fault plane (V_r5, Figure 2e):

$$V_r 4\,(\mathrm{dis}) = \mathrm{dis} \cdot 0.035 + 0.6 \cdot V_s \qquad (V_r(d) \le 0.92\ V_s) \qquad (1)$$

$$V_r 5(x,\ y) = (0.32 \cdot (D(x,\ y)/\mathrm{Dmax})^{\ 2} + 0.6) \cdot V_s \qquad (2)$$

where D_{max} is the maximum slip reached on the fault plane and (x,y) are the local coordinates on the fault. We decrease the slip on the upper part of the fault to avoid super-shear condition of the rupture velocities.

The rupture velocity described in Equation (1) is derived from dynamic spontaneous modeling (Ohnaka and Shen, 1999): at larger distances from the nucleation, the dynamic loading of the breaking points increases and hence accelerates the rupture front; the constant parameters in the equation are chosen to fix a minimum velocity value at zero distance and to ensure a slowly growing of rupture velocity. The variable rupture velocity defined in Equation (2) is based on modifying the formulation of Ruiz (2007) using a 2nd order dependence of V_r on the total slip, in order to avoid the generation of strong stopping phases.

The source model of Irpinia mainshock, inferred from the inversion of strong motion data (Cocco and Pacor, 1993) is characterized by two main asperities (Slip A of Figure 2), with the position of the nucleation point corresponding to the instrumental hypocenter (40.76N, 15.31E, depth of 15km, NP=*a* in Figure 2; Working group ITACA, 2008) and producing a quasi-unilateral rupture propagation toward northwest.

Shaking scenarios and sensitivity of peak ground motion to kinematic source parameters

The number of simulated scenarios at bedrock, resulting from different choices of rupture parameters, leads to 420 three-component time series at each site, both in displacement and velocity. Spectral displacement with 5% damping ratio (SD) and peak velocity values (PGV) are derived from the geometric mean of the horizontal components.

We first examine the reliability of our ground-motion simulations by comparing the SD values at 2 seconds at all sites as a function of fault distance R_{JB} with the AB07 (Akkar and Bommer, 2007) ground motion predictive equation (GMPE), derived from European/Middle East strong-motion records (Figure 4). Other empirical equations for response spectra, using the same distance metrics, give similar results for the chosen period (Boore and Atkinson, 2008; Bommer et al., 2009). The chosen period (T=2s) defines the beginning of the constant displacement range of the spectrum (CEN, 2004), it allows the comparison with the data recorded during the 1980 Irpinia earthquake (not reliable at periods larger than 3-5 s; ITACA Working Group, 2008) and it is within the frequency range used in this study.

The mean values of the simulated motions combining all scenarios follow very well the AB07 mean prediction (Figure 4a). Moreover, the majority of the recorded data are within one standard deviation of the synthetics and of the AB07 equation. The ground motion experienced at Sturno (STU) is controlled by the maximum directivity effect and is simulated by the synthetic scenarios producing the extreme values; BIS, instead, is classified as rock site but it is affected by site effects due to a velocity inversion (clay shale formation underlying the conglomerate slab; Olivares and Silvestri, 2001), not simulated in our synthetics.

To quantify the comparison with the empirical model, we computed the residuals of the logarithmic SD values between the empirical estimates obtained from AB07 (Akkar and Bommer, 2007) and the simulations (residual = $\log_{10}$[SD_AB07] − $\log_{10}$[SD_synthetic], Figure 4b). The standard deviation of the residuals is comparable with the empirical standard deviation (gray bars in Figure 4b).

The sites with the same fault distance R_{JB} can experience very different variability (e.g. BAG and st02) due to different azimuth, and the larger standard deviations are associated to sites in the strike direction (Figure 4a) where forward and backward directivity effects are stronger.

Figure 5 shows the spatial distribution of the directivity correction factor defined by Spudich and Chiou (2008) overlapping the SD values averaged over all the computed scenarios at each site (black circles). SD values at sites on the foot-wall position are larger than hanging-wall ones. This

feature is mainly due to the combined effects (called "directivity" in the engineering literature) of prevailing up-dip rupture propagation, source-to-receiver geometry and earthquake source radiation pattern (Spudich and Chiou, 2008). The coefficient proposed by Spudich and Chiou (2008) to calculate a directivity correction factor to the ground motion prediction equations, qualitatively explains the spatial variation of the simulated data: i) directivity effects increase the values in the up-dip direction; ii) the sites in the foot-wall falling in the positive area of the coefficient, iii) while the synthetic mean values at sites located on the hanging wall are strongly lowered by the S-wave nodal plane of the radiation pattern (Figure 5).

To investigate the source of variability in the synthetic values, we analyze the distributions of peak ground motion obtained from all shaking scenarios at each site and we examine which is the contribution of each kinematic source parameter to the peak distribution. Figure 6 shows the histograms of SD at 2s for four sites, selected to sample spatial regions of possible different ground motion behavior due to the fault-to-site position and to the directivity effects: BAG (Bagnoli), Pote (Potenza), st02 and st09 (Figure 1 and Figure 5). The shape of the obtained distributions is consistent with the log-normal distribution expected from the empirical model for bedrock sites.

Because in this study the whole variability of the simulated intensity measures is referred to the source rupture modeling, we show in Figure 7 how different choices of nucleation point (panel a), rupture velocity (panel b), source time function (panel c) and slip model (panel d) affect the SD values expected at a single site (BAG for all the studied kinematic source parameter and st02 only for the nucleation point). The sensitivity of ground motions to kinematic source parameters depends on the source parameter itself; for example, the different positions of rupture initiation (NP) have large influence: site st02 (panel a1 of Figure 7) experiences decreasing SD values as the nucleation point moves from *a* to *g* position (Figure 1), i.e. the lowest SD is observed when the earthquake nucleates close to the fault edge adjacent to the site and the rupture front moves far from it (nucleation point *g* in panel a1, Figure 7); conversely at BAG site (panel a2 of Figure 7) the nucleation points located at the eastern positions on the fault plane (Figure 1) contribute to the lowest values, while the central nucleation points produce an increase of the SD. These results can be explained in terms of directivity effects; the position of nucleation point causes a rupture front that propagates backward or forward to the site.

The directivity effect also explains the strong dependence of SD values on the five rupture velocities, Vr (panel b of Figure 7): the SD increases as the constant rupture velocity increases (rupture velocity V_r3 contributes to the highest values). Moreover, the Vr4 rupture velocity produces a distribution similar to the constant rupture velocity Vr1 (2.1 km/s) but with smaller variability; in fact, the average velocities along strike and dip directions are 1.82-2.26 km/s and

1.94-1.98 km/s, respectively, depending on the nucleation position. Similar behavior is observed for Vr5.

The different source time functions, STF (panel *c* of Figure 7), give similar shapes of the distributions. Moreover, the regularized Yoffe and cosine functions yield the highest values of SD. This feature is due to the spectral (Figure 3) and dynamic properties of these two source time functions, whose slip velocities have a larger high-frequency content than for the boxcar and exponential functions and contribute to the maximum values of the simulated ground motion.

Finally, the slip models B and C produce higher motion than model A because the slip patches are closer to the selected site BAG (panel *d* in Figure 7).

Scenario selection

The statistical distributions of ground motion parameters can help for the selection of shaking scenarios whose characteristics follow defined criteria. A typical example is the choice of a subset of scenarios whose peak value or spectral ordinates match a given value inferred from empirical predictive models, from probabilistic seismic hazard analysis (CEN 2004) or directly from the distribution itself. In this case it is possible to select the scenarios which produce the modal value (maximum probability of occurrence), or the extreme value, or mean value, or the percentiles of the distribution inferred from the histograms. This approach is similar to the de-aggregation of seismic hazard for extracting those scenarios that contribute most to the seismic hazard at a given site.

In general, there is more than one scenario giving similar values of the selected ground motion parameter at one site. As an example, Figure 8 shows the distributions of SD at 2s and PGV for BAG site. Three different groups of shaking scenarios are highlighted: group I, which collects the ensemble of scenarios producing the maximum probability of SD occurrence within ±10% of the total range (42% of all scenarios), group II and group III, representing the ensemble of scenarios within the 20% of the total range below the maximum value of SD (4% of all scenarios) and of PGV (3% of all scenarios), respectively.

The selected scenarios are characterized by different combination of kinematic rupture parameters and for each group we can separate the contribution of rupture velocity, slip model, nucleation point and source time function. Scenarios belonging to group I (maximum probability of occurrence of SD at 2s, Figure 8b) mostly depend on the lowest rupture velocities (V_r1, V_r4 and V_r5), and there is a slightly dependence on the boxcar and exponential source time functions (Figure 3) and on the nucleation points located towards the fault edges. On the contrary, scenarios of group II (maximum SD values, Figure 8c) are characterized by the largest rupture velocity (V_r3), slip model B and C

having the slip patches close to the site, nucleation points in the directive position (*c* and *d*) and the cosine and regularized Yoffe source time functions, which have a larger high frequency content (Figure 3 and Figure 7d).

The scenario selection can require a combination of several conditions to be satisfied (e.g., Bazzurro and Cornell, 2002). As an example, we should look for the scenarios simultaneously producing a given value of two ground motion parameters (such as SD and PGV) at the same site (Figure 8), or a given value of spectral displacement at two sites with the same fault distance.

The first example regards the selection of scenarios producing the maximum value of both SD at 2s and PGV at the site BAG (group II and III, Figure 8); this is necessary, for example, when a seismic response study is performed on different type of structures at the same location. These scenarios are characterized by the maximum rupture velocity (V_r3) and by the slip distributions B or C (Figures 8c and 8e). However, a smaller number of nucleation points contributes to the maximum PGV, leading to 10 common set of rupture parameters producing both maximum SD and PGV.

In the case of earthquake scenarios for extended areas (such as an urban district), the selection of a scenario whose peak values are the same at more then one site (multiple sites selection) is not straightforward, especially for sites in near source region. As an example, we select the two sites BAG and st02, which have the same fault distance (Rfault ~ 7 km) but different azimuth (Figure 1). The scenarios producing the spectral values expected from the AB07 empirical predictive model (SD±5%=0.099±0.005 m; Akkar and Bommer, 2007) are the 6% and 4% of the simulated scenarios for BAG and st02, respectively. Among the selected scenarios, only 3 of them (0.7% out of 420 scenarios) have same rupture velocity (Vr2,Vr3 and Vr5), slip (model A, B and C) and nucleation point (*b* and *d*). However, none of the rupture models producing maximum spectral displacement at both BAG and st02 sites have the same source time function; this means that there is not a common set of rupture parameters producing similar SD at two sites with the same fault distance.

Discussion

With the increasing use of non-linear analysis techniques in the seismic design of structures, the prediction of ground motion time series has become indispensable for the complete determination of structural response and damage estimation for future large earthquakes.

The use of synthetic approach may also help us to study the variability of the strong ground motion (e.g. Andrews et al., 2007; Søresen et al., 2007) and to infer a robust classification of the ground motion based on the source parameters describing the rupture process, which are in general affected by the uncertainties on the kinematic source parameters (Irikura et al., 2004).

Our work aims at contributing to this open debate, with the main objectives of studying and quantifying the effect of kinematic source variability on the ground motion parameters. We have modeled scenarios for a fault mechanism similar to the 1980 Irpinia, Italy, earthquake source (Mw 6.9), using a discrete wave-number/finite element technique to compute the full-wave displacement and velocity time series in the zero-to-intermediate frequency band. We have used a massive computation of synthetic seismograms at several sites located in the near-source region, resulting from hundreds of rupture models with different combination of rupture velocity, nucleation position, source time function and slip distribution. The values of the rupture parameters were chosen within a range defined in previous studies, depending on the degree of knowledge of the physical mechanisms controlling the process and accounting for the correlation between them (like high slip is associated to higher-than-average rupture speed). The obtained shaking scenarios, including the worst case scenario (Andrews et al., 2007), represent a set of possible earthquakes which may rupture the same seismogenic fault. The same approach described in this study can be applied to study other source-to-receiver geometry, magnitude and style of faulting.

We chose two intensity measures which account for different characteristic of the ground motion: spectral displacement of 5% damping at 2 s and the peak ground velocity.

Kinematic source parameters have a significant influence on the resulting ground motions, either in terms of mean values or of the shape of the ground motion distributions. We have shown how peak distributions depend on both azimuth and distance, changing significantly in shape and mean values with the position of the recording site with respect to the fault. The decrease with distance of the peak ground motion is not isotropic in the near source range and the azimuthal variability depends on the rupture model, whereas the majority of the ground motion predictive equations assume an isotropic behavior.

The analysis of the effect of the source parameters on the ground motion scenarios may be used to reduce the number of simulations by varying only those rupture parameters which mostly contribute to a specific ground motion measure or which are likely to give values of interest for the particular case study.

However, the large amount of synthetic data provides a detailed description of the variability that could be observed at a given site, or at several sites, for different earthquakes. This variability can largely affect the scenario prediction and it should be considered when dealing with damage assessment in urban areas or for large structures (Ansal et al, 2009). For these studies it is important to access to synthetic database including different intensity measures and whose values have a specific significance (e.g. associated to mean motions, all simulation results, 84% percentile, etc.). We have then used the histograms of the simulated ground motion parameters to select one or more

representative rupture scenarios matching specific properties in terms of peak or spectral ordinates values at a given site. In this case the same intensity value can be related to seismograms generated by different rupture models; in other word, seismograms with the same peak value can be produced by different possible earthquakes on the fault and may have different characteristics in terms of frequency content and duration (Figure 9). Moreover, it can be possible to select seismograms satisfying more than one ground motion parameter (e.g., given values of SD and PGV simultaneously), even though it is not always possible to select a scenario satisfying more than one request. This quantitative selection procedure may be useful for finding several temporal signals to be used, for example, in the dynamic analysis of structures.

The present study contributes to improve our understanding on the seismic source and on its effects on the ground motion predictions, even though the behavior of the peak ground motion distributions depends on the specific fault and site configuration and cannot be "extrapolated" to other geometries.

Many efforts are still needed to improve our ability to accurately estimate the most critical source parameters influencing the ground motion; a robust evaluation of the kinematic source parameters, not only in terms of mean value but also in terms of distribution functional shape as well as its range limits, is essential to define ground shaking scenarios for seismic-hazard assessment and risk analysis, along with a correct modeling of the variation on propagation wave path. However, we believe that seismologists can give a large contribution to the seismic engineering studies by reproducing and explaining the large variability of expected ground motion in the near source region.

Data and Resources

The Simulations presented in this article were partially performed within the project, Scenari di scuotimento in aree di interesse prioritario e/o strategico (Shaking seismic scenarios in area of strategic and/or priority interest), promoted in the period 2004–2006 by the Italian Civil Protection and INGV (http://esse3.mi.ingv.it, last accessed on July 2009). The deliverables relevant to the simulation techniques (task 1) are Deliverable D0, Simulation techniques, and D1, Guidelines to compute shaking scenarios (in Italian) (http://esse3.mi.ingv.it/S3_del.php, last accessed on July 2009).

The seismograms recorded duringa the 1980 Irpinia earthquake come from the Accelerometric Italian Network (ITACA Working Group, 2008).

Acknowledgments

We thank the associated editor Gail Atkinson and the three reviewers (J. Douglas, M. Mai and an anonymous referee) for the thoughtful review. All the criticisms have been useful to clarify and focus the results of the paper.

We also want to acknowledge G. Ameri, A. Emolo, F. Gallovic, P. Spudich and D. Boore for the deep and fruitful discussions which highly improved the quality of the results.

This work started during the Italian Project S3 "Shaking seismic scenarios in area of strategic and/or priority interest" (http://esse3.mi.ingv.it/index.htm), funded by the Italian *Dipartimento della Protezione Civile* in the frame of the 2004-2006 Agreement with *Istituto Nazionale di Geofisica e Vulcanologia* (INGV). Last development has been carried out under the financial auspices of the Italian Ministry for Research and Higher Education (MiUR - Ministero dell'Università e della Ricerca) through the FIRB Project No RBIN047WCL (Assessment and Reduction of Seismic Risk to Large Infrastructural Systems).

References

Amato, A., and Selvaggi G. (1993). Aftershock location and P-velocity structure in the epicentral region of the 1980 Irpinia earthquake. *Annali di Geofisica*, 36, 3-15.

Ambraseys, N., P. Smith, R. Berardi, D. Rinaldis, F. Cotton, and C. Berge-Thierry, (2000). Dissemination of European strong-motion data [CD-ROM], Eur. Counc., Environ. and Clim. Res. Program, Brussels, Belgium.

Ameri, G., Akinci A., Cocco M., Cultrera G., Franceschina G., Pacor F., Pessina, V., Lombardi A.M., (2007). Ground motion scenario for selected cities (pp 41-58). In: Technical dissemination N. 8 SP11 - Prediction of ground motion and loss scenarios for selected infrastructure systems in European Urban Environment/ (Eds: Faccioli E.) IUSS Press, ISBN 978-88-6198-012-9, pp. 210.

Ameri, G., Pacor, F., Cultrera, G. and G. Franceschina (2008). Deterministic Ground-Motion Scenarios for Engineering Applications: The Case of Thessaloniki, Greece. *Bull. Seism. Soc. Am.*, **98**, 3, 1289–1303.

Andrews, D. J. (1976). Rupture velocity of plane strain shear cracks, *J. Geophys. Res.*, 81, No. 32, 5679-5687

Andrews, D. J. (1980). A stochastic Fault Model 1. Static case, *J. Geophys. Res.*, **85**, 3867-3877.

Andrews, D.J., T. C. Hanks, and J.W. Whitney (2007). Physical limits on ground motion at Yucca Mountain, *Bull. Seism. Soc. Am.*, 97, 1771-1792.

Ansal A., A. Akinci, G. Cultrera, M. Erdik, V. Pessina, G. Tonuk, G. Ameri, (2008). Loss estimation in Istanbul based on deterministic earthquake scenarios of the Marmara Sea region (Turkey). *Soil Dynamics and Earthquake Engineering*, in press. Available online 30 August 2008.

Aochi H. and J. Douglas, (2006). Testing the Validity of Simulated Strong Ground Motion from the Dynamic Rupture of a Finite Fault, by Using Empirical Equations. Bulletin of Earthquake Engineering (2006) 4:211–229, DOI 10.1007/s10518-006-0001-3

Aki K. and P.G. Richards, (2002). Quantitative Seismology: Theory and Methods, second edition. University Science Books.

Akkar, S, Bommer, JJ, Prediction of elastic displacement response spectra in Europe and the Middle East, Earthq. Eng. Struct. D., 2007, Vol: 36, Pages: 1275 - 1301, ISSN: 0098-8847

Baker J. W. and C. A. Cornell, (2006). Vector-Valued Ground Motion Intensity Measures for Probabilistic Seismic Demand Analysis. PEER Report 2006/08, Pacific Earthquake Engineering Research Center-College of Engineering, University of California, Berkeley.

Bazzurro P., Cornell C.A., 2002. Vector-valued probabilistic seismic hazard analysis. The Seventh U.S. National Conference on Earthquake Engineering, Boston, MA.

Bernard P., A. Herrero, and C. Berge, (1996). Modeling directivity of heterogeneous earthquake ruptures *Bull. Seism. Soc. Am.*, 86, 1149-1160.

Beroza, G. C., and P. Spudich. 1988. Linearized Inversion for Fault Rupture Behavior - Application to the 1984 Morgan-Hill, California, Earthquake. J. Geophys. Res., 93 (B6):6275-6296.

Birgören, G., Sekiguchi H., and K. Irikura, (2004). Rupture model of the 1999 Duzce, Turkey, earthquake deduced from high and low frequency strong motion data. *Geoph. Res. Lett.*, 31, L05610, doi:10.1029/2003GL019194.

Bizzarri, A., Cocco M., Andrews D. J., Boschi E., (2001). Solving the dynamic rupture problem with different numerical approaches and constitutive laws. *Geophys. J. Int.* 144, 656-678.

Bizzarri, A., and P. Spudich (2008), Effects of supershear rupture speed on the high-frequency content of S waves investigated using spontaneous dynamic rupture models and isochrone theory, *J. Geophys. Res.*, 113, B05304, doi:10.1029/2007JB005146.

Bommer JJ, NA Abrahamson, (2006). Why Do Modern Probabilistic Seismic-Hazard Analyses Often Lead to Increased Hazard Estimates? *Bull. Seism. Soc. Am.*, 96; 6; 1967-1977; DOI: 10.1785/0120060043

Bommer JJ, Alarcón JE (2006) The prediction and use of peak ground velocity. J Earthq Eng 10(1):1–31. doi:10.1142/S1363246906002463

Bommer, JJ, Stafford, PJ, Akkar, S, Current empirical ground-motion prediction equations for Europe and their application to Eurocode 8, Bulletin of Earthquake Engineering, 2009, Published online: 28 May 2009. DOI: 10.1007/s10518-009-9122-9

Boore, D. M. and G. M. Atkinson (2008). Ground-motion prediction equations for the average horizontal component of PGA, PGV, and 5%-damped PSA at spectral periods between 0.01 s and 10.0 s, Earthquake Spectra 24, 99--138.

Bouchon, M. Bouin, M.-P. Karabulut, H. Toksoz, M. N. Dietrich, M.; Rosakis, A. J., (2001). How Fast is Rupture during an Earthquake? New Insights from the 1999 Turkey Earthquakes, *Geoph. Res. Lett*., 28, 14, 2723-2726.

Bouchon M., M. N. Toksöz, H. Karabulut, M.-P. Bouin, M. Dietrich, M. Aktar and M. Edie, (2002). Space and Time Evolution of Rupture and Faulting during the 1999 Izmit (Turkey) Earthquake. *Bull. Seism. Soc. Am.*, 92; 1; 256-266; DOI: 10.1785/0120000845.

Causse M., F. Cotton, C. Cornou, and P.-Y. Bard, (2008). Calibrating Median and Uncertainty Estimates for a Practical Use of Empirical Green's Functions Technique. *Bull. Seism. Soc. Am.*, 98, 1, 344–353, doi: 10.1785/0120070075

CEN (2004). Eurocode 8: Design of structures for earthquake resistance - Part 1: General rules, seismic actions and rules for buildings. *Bruxelles*.

Cirella, A., A. Piatanesi, E. Tinti and M. Cocco (2006). Dynamically consistent source time functions to invert kinematic rupture histories. *Eos, Trans. AGU 87*(52), Fall Meet. Suppl., Abstract S41B-1323.

Cirella, A., A. Piatanesi, E. Tinti, and M. Cocco, (2008). Rupture process of the 2007 Niigata-ken Chuetsu-oki earthquake by non-linear joint inversion of strong motion and GPS data. *Geophys. Res. Lett.*, 35, L16306, doi:10.1029/2008GL034756.

Cohee, B. P., and G. C. Beroza, (1994). Slip distribution of the 1992 Landers earthquake and its implications for earthquake source mechanics. *Bull. Seismol. Soc. Am.*, 84, 693–712.

Convertito V. and A. Herrero (2004). Influence of focal mechanism in probabilistic seismic hazard analysis. *Bull. Seism. Soc. Am.*, 94, 2124-2136.

Convertito V., A. Emolo and A. Zollo (2006). Seismic hazard assessment for a characteristic earthquake scenario: an integrated probabilistic – deterministic method. *Bull. Seism. Soc. Am.*, 96, No. 2, 377-391, doi: 10.1785/0120050024.

Custódio, S., and R. J. Archuleta (2007). Parkfield earthquakes: Characteristic or complementarity?. *J. Geophys. Res.*, 112, B05310, doi: 10.1029/2006JB004617.

Das, S. and Aki, K. (1977). A numerical study of two-dimensional spontaneous rupture propagation. *Geophys. J. R. Astr. Soc.*, 50, 643-668.

Day, S. (1982). Three-dimensional finite-difference simulation of fault dynamics: rectangular faults with fixed rupture velocity. *Bull. Seismol. Soc. Am.*, 72, 705-727.

Delouis, B, Giardini D., Lundgren P. and Salichon J. (2002). Joint inversion of Insar, GPS, teleseismic and strong-motion data for the spatial and temporal distribution of earthquake slip: application to the 1999 Izmit mainshock. *Bull. Seismol. Soc. Am.*, 92(1), 278-299.

Frankel, A. (1991). High-frequency spectral falloff of earthquakes, fractal dimension of complex rupture, b value, and the scaling of strength on fault, *J. Geophys. Res.*, **96**, 6291-6302.

Guatteri M., Mai P.M., and Beroza G.C., (2004). A pseudo-dynamic approximation to dynamic rupture models for strong ground motion prediction. Bull. Seis. Soc. Am., 94,6,2051-2063

Hanks, T. (1979). b values and w^g seismic source models : implications for tectonic stress variations along active crustal fault zones and the estimation of high frequency strong ground motion', *J. Geophys. Res.*, **84**, 2235-2242.

Harris R.A. and J. R. Arrowsmith, (2006). Introduction to the Special Issue on the 2004 Parkfield Earthquake and the Parkfield Earthquake Prediction Experiment. *Bull. Seism. Soc. Am*, 96, 4B, 1-10, doi: 10.1785/0120050831

Herrero A. e P. Bernard (1994). A kinematic self-similar rupture process for earthquakes. *Bull. Seism. Soc. Am.*, 84, 1216-1228.

Heaton, T. H. (1990). Evidence for and implication of self-healing pulses of slip in earthquake rupture. *Phys. Earth Planet. Int.*, 64, 1-20.

Improta L., M. Bonagura, P. Capuano and G. Iannaccone (2003). An integrated geophysical investigation of the upper crust in the epicentral area of the 1980, Ms=6.9, Irpinia earthquake (Southern Italy). *Tectonophysics*, 361,1-2, pp.139-169.

Irikura K., H. Miyake, T. Iwata, K. Kamae, H. Kawabe, and L. A. Dalguer, (2004). Recipe for predicting strong ground motions from future large earthquakes. Proceedings of the *13th World Conference on Earthquake Engineering*, Vancouver (B.C., Canada), August 2004, Paper No. 1371.

ITACA Working Group (2008) - Data Base of the Italian strong motion data: http://itaca.mi.ingv.it

Joyner, W.B. and Boore, D.M. (1981). Peak horizontal acceleration and velocity from strong-motion records including records from the 1979 Imperial Valley, California, earthquake. *Bull. Seism. Soc. Am.*, 71(6), 2011–2038.

Liu, P., and R. Archuleta (2004). A new nonlinear finite fault inversion with three-dimensional Green's functions: application to the 1989 Loma Prieta, California, earthquake. *J.Geophys. Res.*, 109, B02318, doi:10.1029/2003JB002625.

Ma, K. F., Song, T. R., Lee, S. J. and Wu, H. I. (2000). Spatial slip distribution of the September 20, 1999, Chi-Chi, Taiwan earthquake Mw = 7.6 - inverted from teleseismic data. *Geophys. Res. Lett.*, 27, 3417-3420.

Mai P. M., P. Spudich e J. Boatwright (2005). Hypocenter locations in finite-source rupture models, *Bull. Seism. Soc. Am.*, 95, 965-980.

Manighetti I., M. Campillo, C. Sammis, P. M. Mai, and G. King, (2005). Evidence for self-similar, triangular slip distributions on earthquakes: Implications for earthquake and fault mechanics. *J. Geophys. Res.*, 110.

Manighetti I., G. King, Y. Gaudemer, C. Scholz e C. Doubre (2001). Slip accumulation and lateral propagation of active normal fault in Afar. *J. Geophys. Res.*, 106,13667-13696.

Nielsen S. and R. Madariaga, (2003). On the Self-Healing Fracture Mode. *Bull Seismol Soc Am*, 93:2375–2388.

Oglesby, D. D., R. J. Archuleta, and S. B. Nielsen (2000). The dynamics of dip-slip faulting: explorations in two dimensions, J. Geophys. Res., 105, B6, 13643-13653.

Oglesby, D. D., D. S. Dreger, R. A. Harris, N. Ratchkovski and R. Hansen (2004). Inverse kinematic and forward dynamic models of the 2002 Denali fault earthquake, Alaska. *Bull. Seismol. Soc. Am.*, 94, S214-S233.

Ohnaka M. and L. Shen (1999). Scaling of the shear rupture process from nucleation to dynamic propagation: Implications of geometric irregularity of the rupturing surfaces. *J. Geophys. Res.*, 104, B1, 817–844, 1999.

Olivares L. and F. Silvestri (2001). Analisi della risposta sismica e della subsidenza post-sismica del colle di Bisaccia a seguito del terremoto irpino-lucano del 1980. Proc. X National Conference of Italian National Association of Earthquake Engineering, Potenza-Matera, Italy, 9-13 sept. 2001.

Piatanesi, A., A. Cirella, P. Spudich and M. Cocco (2007). A global search inversion for earthquake kinematic rupture history: Application to the 2000 western Tottori, Japan earthquake. *J. Geophys. Res.*, 112, B07314, doi:10.1029/2006JB004821.

Ripperger J., P. M. Mai, and J.-P. Ampuero, (2008). Variability of Near-Field Ground Motion from Dynamic Earthquake Rupture Simulations. Bulletin of the Seismological Society of America, Jun 2008; 98: 1207 - 1228.

Rodgers, A J, Xie, X, Petersson, A (2007). Bounding Ground Motions for Hayward Fault Scenario Earthquakes Using Suites of Stochastic Rupture Models. S21A-0232, AGU Fall Meeting 2007

Rosakis, A. J. Samudrala, O. Coker, D. (1999). Cracks Faster than the Shear Wave Speed. *Science*, 5418, 1337-1339.

Ruiz J. A. (2007). Modélisation d'accélérogrammes synthétiques large-bande par modélisation de la cinématique de la rupture sismique. PhD thesis, Institut de Physique du Globe de Paris, France.

Sabetta, F., Pugliese, A. (1996). Estimation of response spectra and simulation of non-stationary earthquake ground motion. *Bull. Seism. Soc. Am.*, 86, 337-352.

SCEC/CME CyberShake Project, http://epicenter.usc.edu/cmeportal/CyberShake.html

Sekiguchi H. (2007). Validation of a broadband source modeling method of interplate earthquakes. S34A-06, AGU Fall Meeting 2007

Shakal, A., V. Graizer, M. Huang, H. Haddadi, and K. Lin (2005), Strong-motion data from the M6.0 Parkfield earthquake of September 28, 2004, *Proceedings of SMIP05 Seminar on Utilization of Strong Motion Data, Los Angeles, CA*, 1-18.

Somerville, P. Irikura, K. Graves, R. Sawada, S. Wald, D. Abrahamson, N. Iwasaki, Y. Kagawa, T. Smith, N. Kowada, A., (1999). Characterizing Crustal Earthquake Slip Models for the Prediction of Strong Ground Motion. *Seism. Res. Lett*., 70, 1, 59-80.

Sørensen, B., M., Pulido, N., and Atakan, K., (2007). Sensitivity of Ground-Motion Simulations to Earthquake Source Parameters: A Case Study for Istanbul, Turkey. *Bull. Seism. Soc. Am.*, Vol. 97, No. 3, pp. 881–900, doi: 10.1785/0120060044.

Spudich, P., and Chiou, B.S-J., (2008). Directivity in NGA earthquake ground motions: Analysis using isochrone theory, accepted. *Earthquake Spectra*, 24, 1, 279-298.

Spudich, P., Xu, L., (2002). Documentation of software package Compsyn sxv3.11: programs for earthquake ground motion calculation using complete 1-d green's functions, International Handbook of Earthquake and Engineering Seismology CD, Int. Ass. Of Seismology and Physics of Earth's Interior, Academic Press.

SSN, Servizio Sismico Nazionale Monitoring Systems Group, The strong motion records of Umbria-Marche sequence (September 1997 – June 1998) [CD-ROM], Rome, Italy, 2002.

Tinti E., E. Fukuyama, A. Piatanesi e M. Cocco (2005). A kinematic source-time function compatible with earthquake dynamics. *Bull. Seism. Soc. Am.*, 95, 1211-1223.

Tinti E., Cocco M., Fukuyama E., and Piatanesi A., (2009). Dependence of slip weakening distance (Dc) on final slip during dynamic rupture of earthquakes. Geophys. J. Int., 177,1205-1220.

Wang, H., Igel, H., Gallovic, F., Cochard, A., Ewald, M. (2008). Source-Related Variations of Ground Motions in 3-D media: Application to the Newport-Inglewood Fault, Los Angeles Basin, Geophys. J. Int., 175, 202-214.

Zeng, Y., J. G. Anderson and G. Yu (1994). A composite source model for computing realistic synthetic strong ground motions, *Geoph. Res. Lett.*, 21, 725-728.

Tables and Figures

Table 1. 1D-layered propagation model (Amato and Selvaggi, 1993; Improta et al., 2003; Improta 2009, personal communication). Vs is computed from Vp as Vs=Vp/1.81, and Qs=100.

Figure 1. Stations' location and fault projection with geometry similar to the 1980 Irpinia, Italy, earthquake. Letters *a* to *g* on the fault shows the position of 7 nucleation points, located at 10 km down-dip from the upper edge of the fault and equally spaced along the strike direction (7.0-10.5-14.0-17.5-21.0-24.5-28.0 km, named from *a* to *g* respectively). The line running along the south-west edge of the fault indicates its projection to the surface.

Figure 2. Three distributions of final slip considered in this study, each of them having asperities in different positions: (a) model A, (b) model B, (c) model C. Black contours in panels (d) and (e) represent the rupture fronts associated to the rupture velocity model V_r2 and *Vr5*, respectively, and for nucleation point *#a* (Figure 1); V_r5 depends on the peak slip velocity distribution corresponding to the slip model B.

Figure 3. Source time functions: boxcar (*box*), exponential (*exp*), cosine (*cos*), and regularized Yoffe function with T_{acc}= 0.225s (*yoffe*): (a) in time domain (normalized to unit area); (b) in frequency domain (FFT band-pass filtered between 0 and 2Hz)

Figure 4. Mean horizontal SD (5% damping) at 2s computed at all sites for all simulated scenarios and ordered by fault distance R_{JB} (closest distance to the surface projection of the fault plane). (a) Geometric mean (± 1 standard deviation) at each site and its fit (logSD(R) = -0.5792 * log(R) - 0.5274), compared with the Akkar and Bommer (2007) empirical predictive model for normal faulting (AB2007); gray bars refer to the sites in the strike directions. Stars indicate the same intensity measure as recorded during the first 35 s of the 1980 Irpinia earthquake. (b) Residuals between the empirical estimates from AB07(Akkar and Bommer, 2007) and the simulations; for each site, gray dots are the residual for each scenario and error bars represent the standard deviation compared with the AB07 standard deviation.

Figure 5. Spatial distribution of mean values of SD at 2s averaged over all the computed scenarios at each site (black circles are proportional to the mean value). Gray scale indicates the combined

effect of the directivity and the radiation pattern computed using the definition given by Spudich and Chiou (2008) for the same fault geometry and averaged over the different nucleation point positions.

Figure 6. Histograms of SD for 5% damping at 2s computed for all shaking scenarios at 4 sites; each bin of the histogram is 0.02m. The empirical distributions (lines) are taken from Akkar and Bommer (2007; AB2007); they are computed for the R_{JB} distance of each site and normalized to the total area of the histogram. Arrow at BAG indicates the SD for 5% damping at 2s recorded at the same station during the 1980 Irpinia earthquake (Ambraseys et al., 2000; SSN, 2002).

Figure 7. Distribution of SD for 5% damping at 2s at stations S02 (panel a1) and BAG (panels a2 to d). Color histograms (top plots) represent the cumulative distribution of all scenarios with colors indicating the contribution of a specific kinematic parameter: a) position of nucleation point (NP), b) rupture velocity (Vr), c) source time function (STF), d) slip model (SLIP). Black histograms (single line) on each column represent the distribution of each source parameter alone.

Figure 8. (a) Histograms of SD for 5% damping at 2s and PGV at BAG; gray shades shows three different groups of scenarios: group I (177 scenarios with SD(5%) at 2 s ranging around ±10% of the maximum probability of occurrence), group II (16 scenarios with SD(5%) at 2 s above the 80% of the total range, e.g. 20% below the maximum value),), group III (12 scenarios with PGV above the 80% of the total range, e.g. 20% below the maximum value). The figure displays also the selection of kinematic parameters contributing to the shaking scenarios of (b)group I, (c)group II and (d)group III: rupture velocity (Vr), the total slip (slip), the nucleation point (np) and the source time function (stf).

Figure 9. Example of seismograms computed at BAG, having similar PGV values ranging around the maximum probability of occurrence (PGV =0.41±0.02 m/s) but different rupture models. Four letters code L1-L2-L3-L4 represents: L1= STF (B=box, E=exponential, J=cosine, Y=Yoffe), L2=NP (Figure 1), L3=SLIP (Figure 2) and L4=Vr. The seismograms duration is 30 seconds.

Table 1

Vp (km/s)	Vs (km/s)	ρ (g/cm^3)	Thickness (km)	comments
2.1	1.2	2.2	1	
3.5	1.93	2.3	1	
4.5	2.49	2.5	2	
5.7	3.15	2.6	6	Apula platform
6.5	3.59	2.7	15	
7.5	4.14	2.9	10	
8.1	4.48	3.2	-	Moho

Figure 1

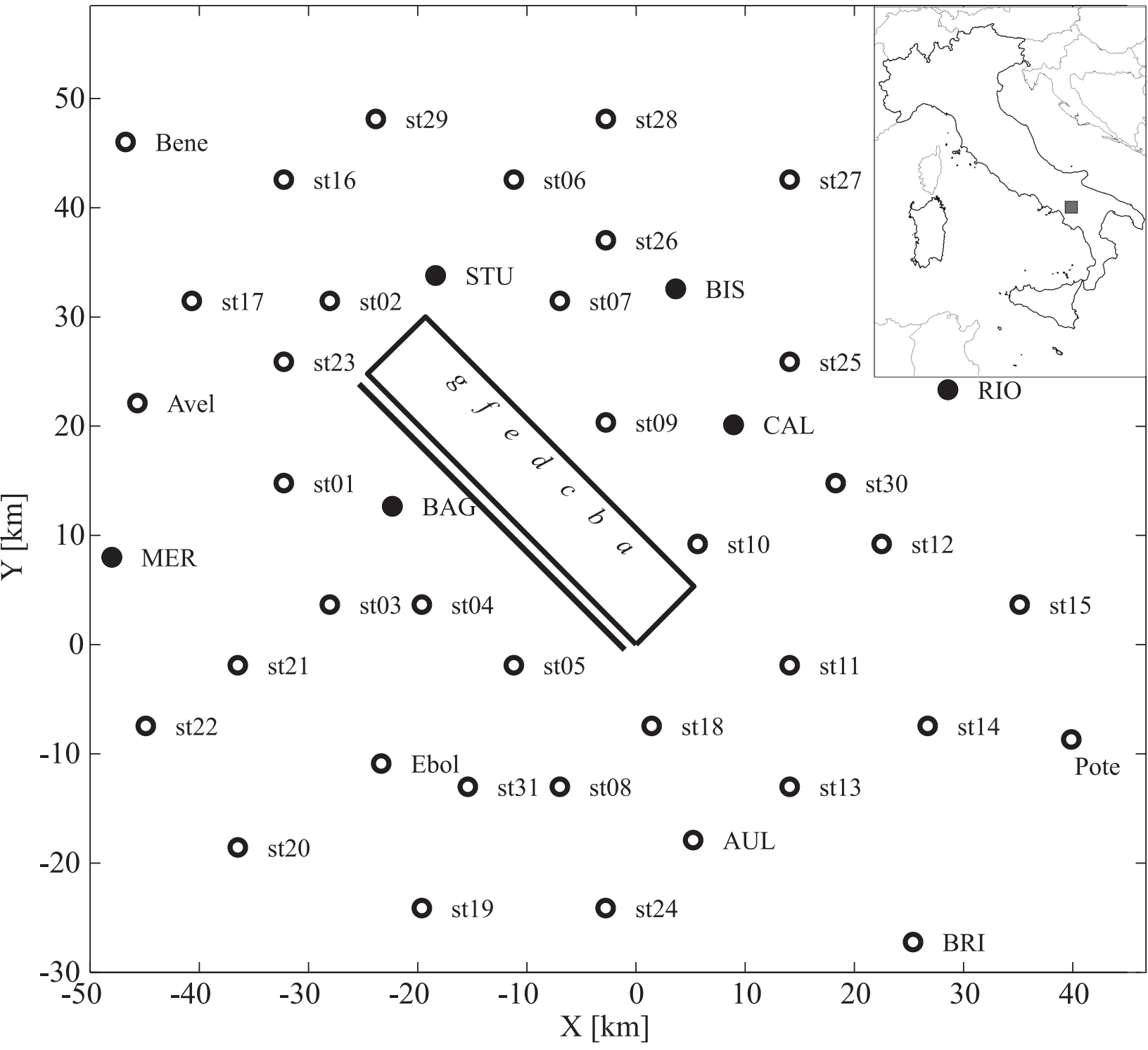
st29
st28
Bene
st16
st06
st27
st26
STU
BIS
st17
st02
st07
st23
st25
RIO
Avel
st09
CAL
st01
st30
BAG
MER
st10
st12
st03
st04
st15
st21
st05
st11
st22
st18
st14
Ebol
Pote
st31
st08
st13
st20
AUL
st19
st24
BRI
g f e d c b a
50
40
30
20
10
0
-10
-20
-30
-50
-40
-30
-20
-10
0
10
20
30
40
Y [km]
X [km]

Figure 2

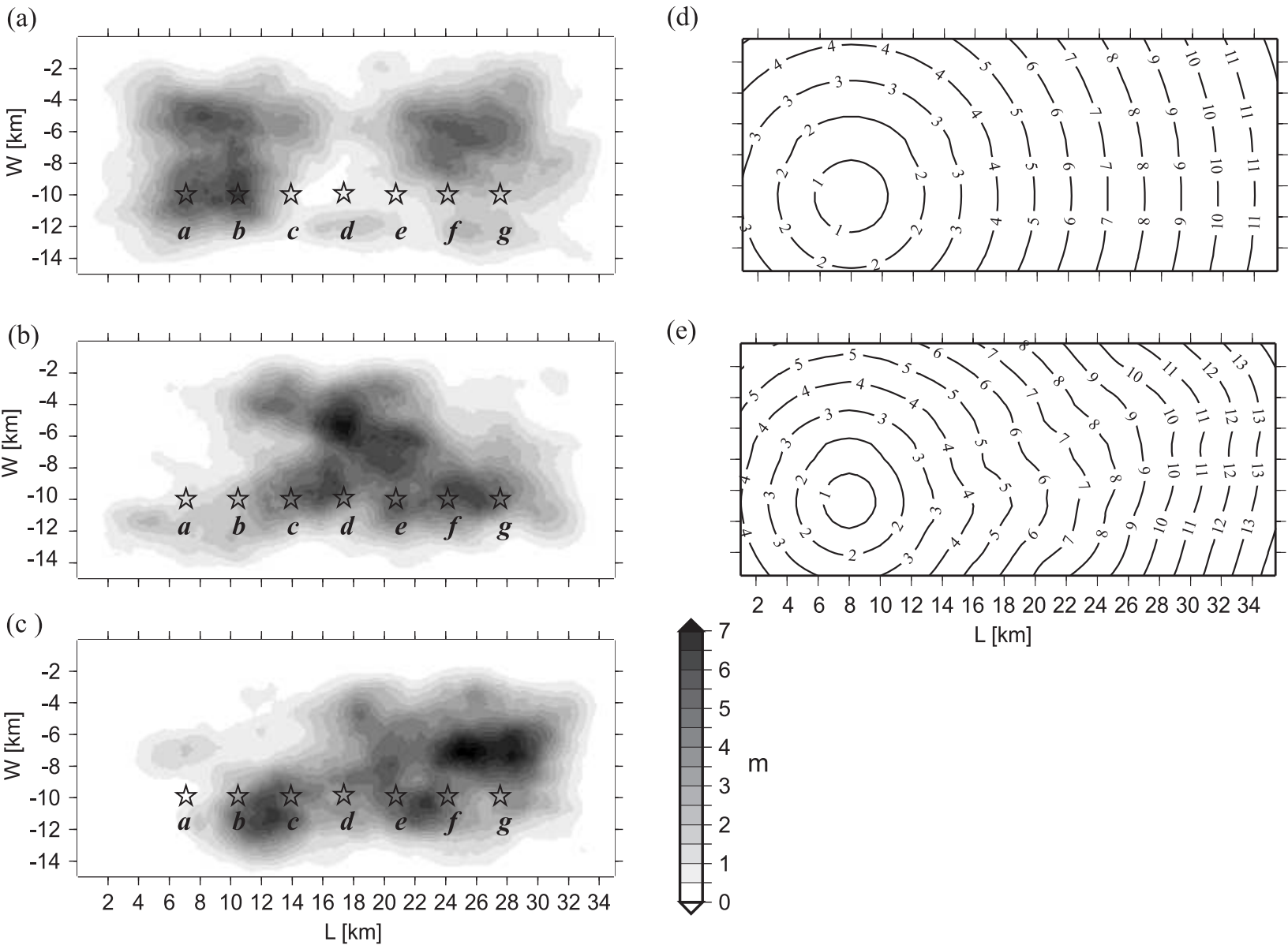
(a)
(b)
(c)
(d)
(e)
W [km]
-2
-4
-6
-8
-10
-12
-14
a
b
c
d
e
f
g
2 4 6 8 10 12 14 16 18 20 22 24 26 28 30 32 34
L [km]
m
0
1
2
3
4
5
6
7

Figure 3

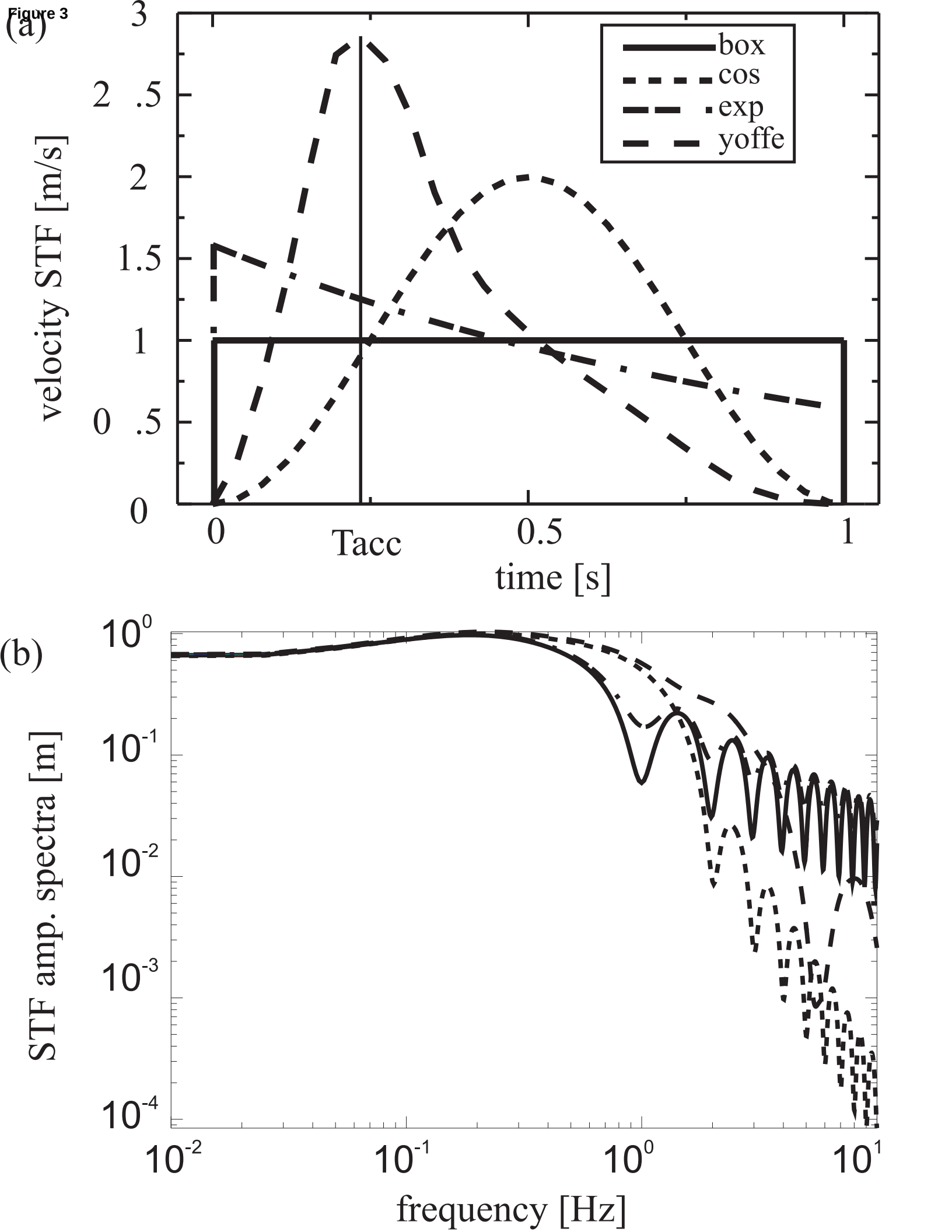
(a)
velocity STF [m/s]
3
2 .5
2
1.5
1
0 .5
0
box
cos
exp
yoffe
0
Tacc
0.5
1
time [s]
(b)
STF amp. spectra [m]
10^{0}
10^{-1}
10^{-2}
10^{-3}
10^{-4}
10^{-2}
10^{-1}
10^{0}
10^{1}
frequency [Hz]

Figure

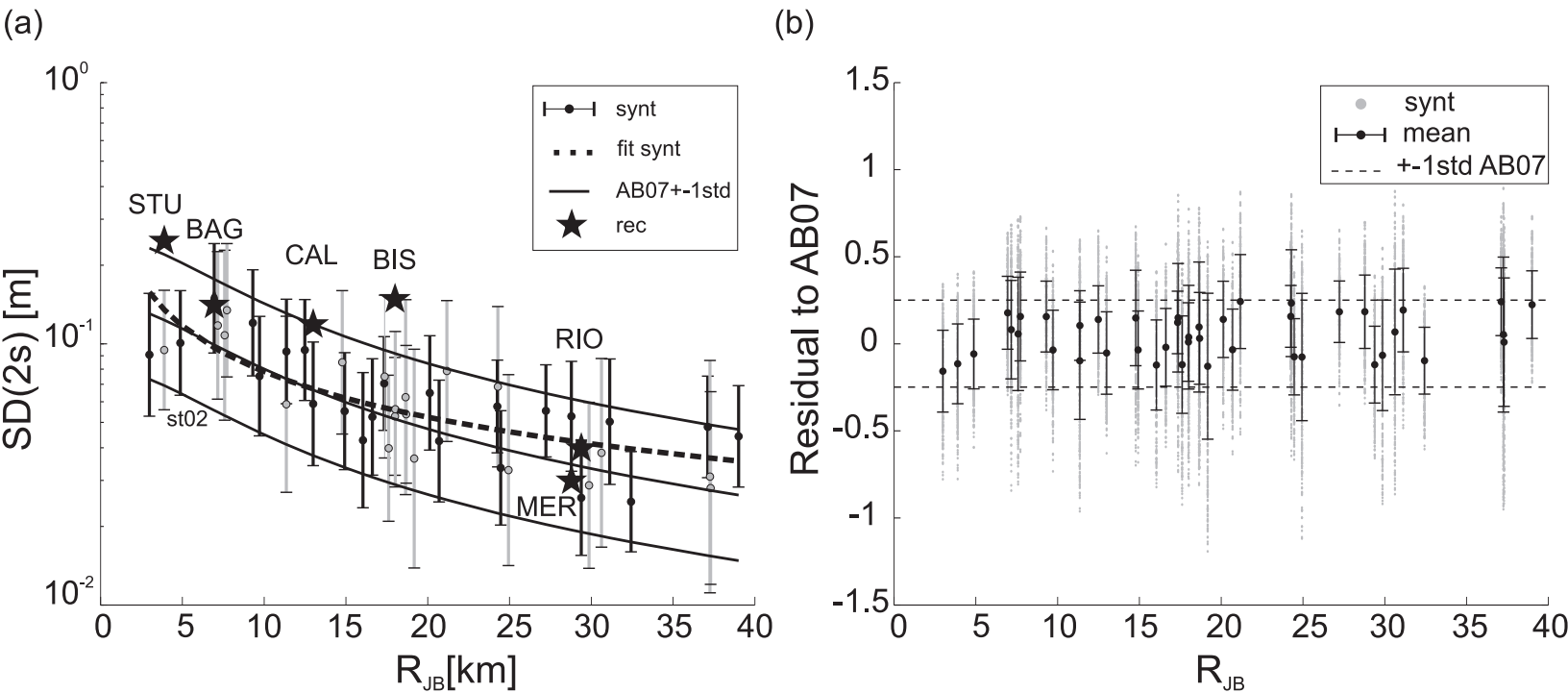
(a)
(b)
synt
fit synt
AB07+-1std
rec
STU
BAG
CAL
BIS
RIO
MER
st02
SD(2s) [m]
R_{JB}[km]
Residual to AB07
mean
+-1std AB07
R_{JB}

Figure 5

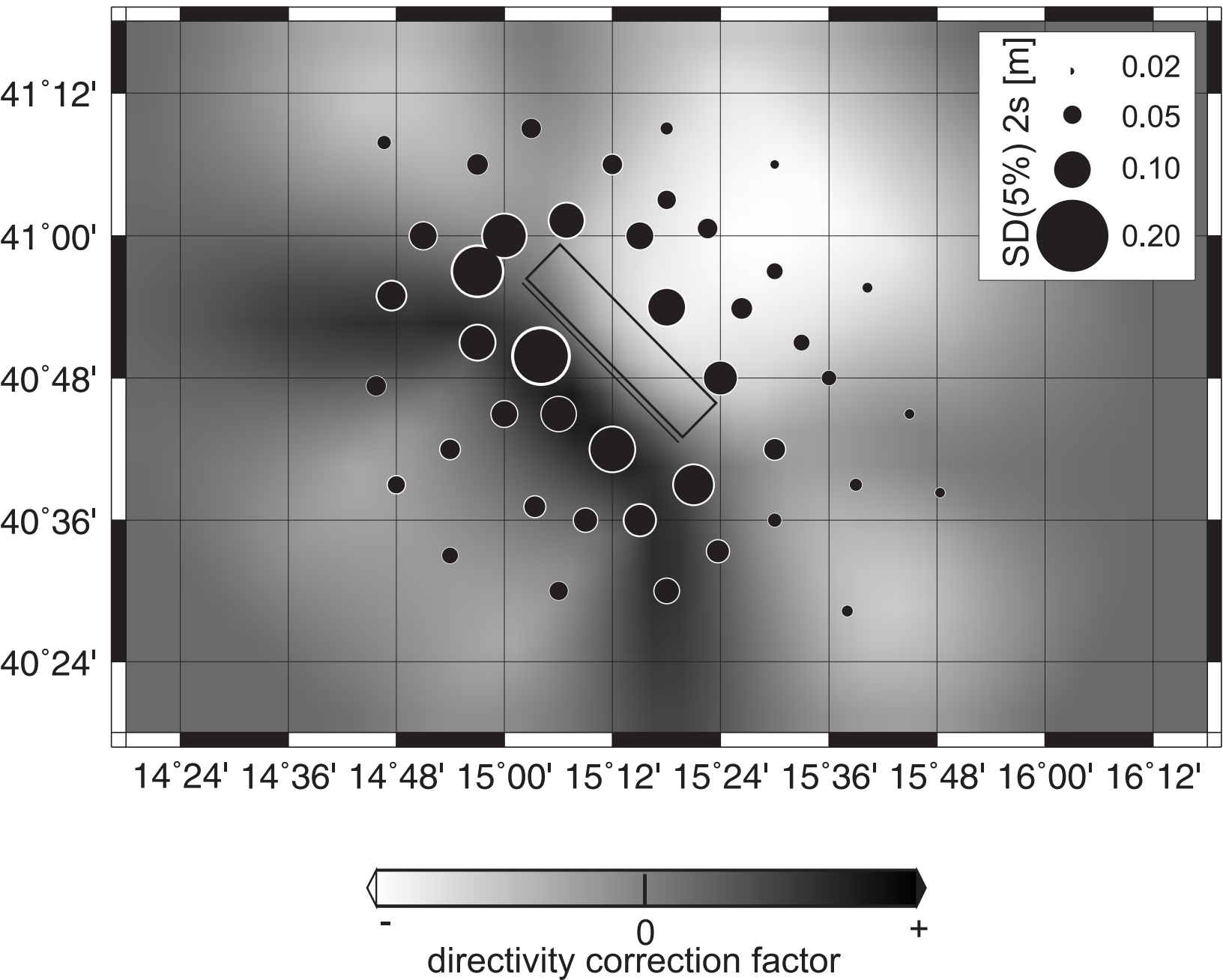
41˚12'
41˚00'
40˚48'
40˚36'
40˚24'
14˚24' 14˚36' 14˚48' 15˚00' 15˚12' 15˚24' 15˚36' 15˚48' 16˚00' 16˚12'
SD(5%) 2s [m]
0.02
0.05
0.10
0.20
-
0
+
directivity correction factor

Figure 6

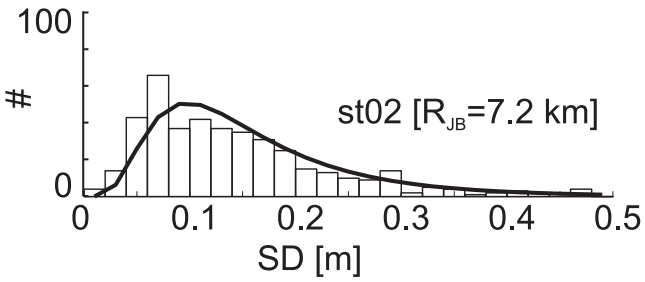
100
#
0
st02 [R_JB=7.2 km]
0
0.1
0.2
0.3
0.4
0.5
SD [m]

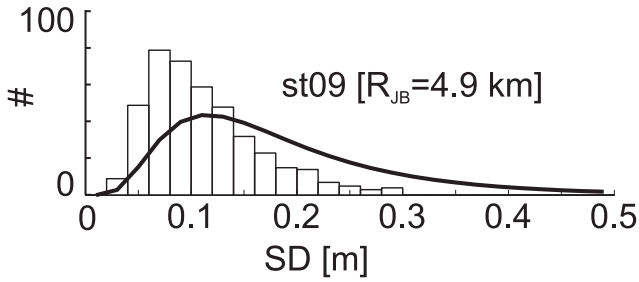
100
#
0
st09 [R_JB=4.9 km]
0
0.1
0.2
0.3
0.4
0.5
SD [m]

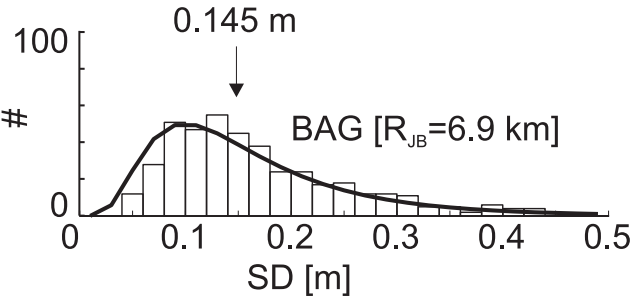
0.145 m
100
#
0
BAG [R_JB=6.9 km]
0
0.1
0.2
0.3
0.4
0.5
SD [m]

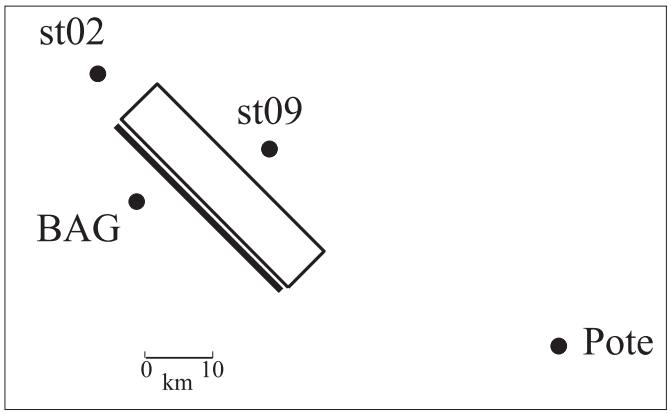
st02
st09
BAG
Pote
0 km 10

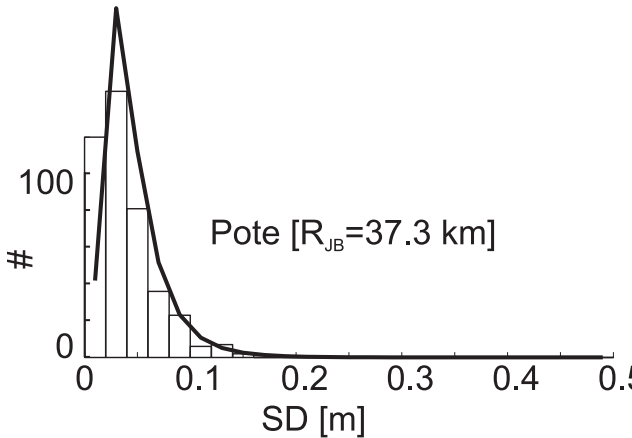
100
#
0
Pote [R_JB=37.3 km]
0
0.1
0.2
0.3
0.4
0.5
SD [m]

Figure 7

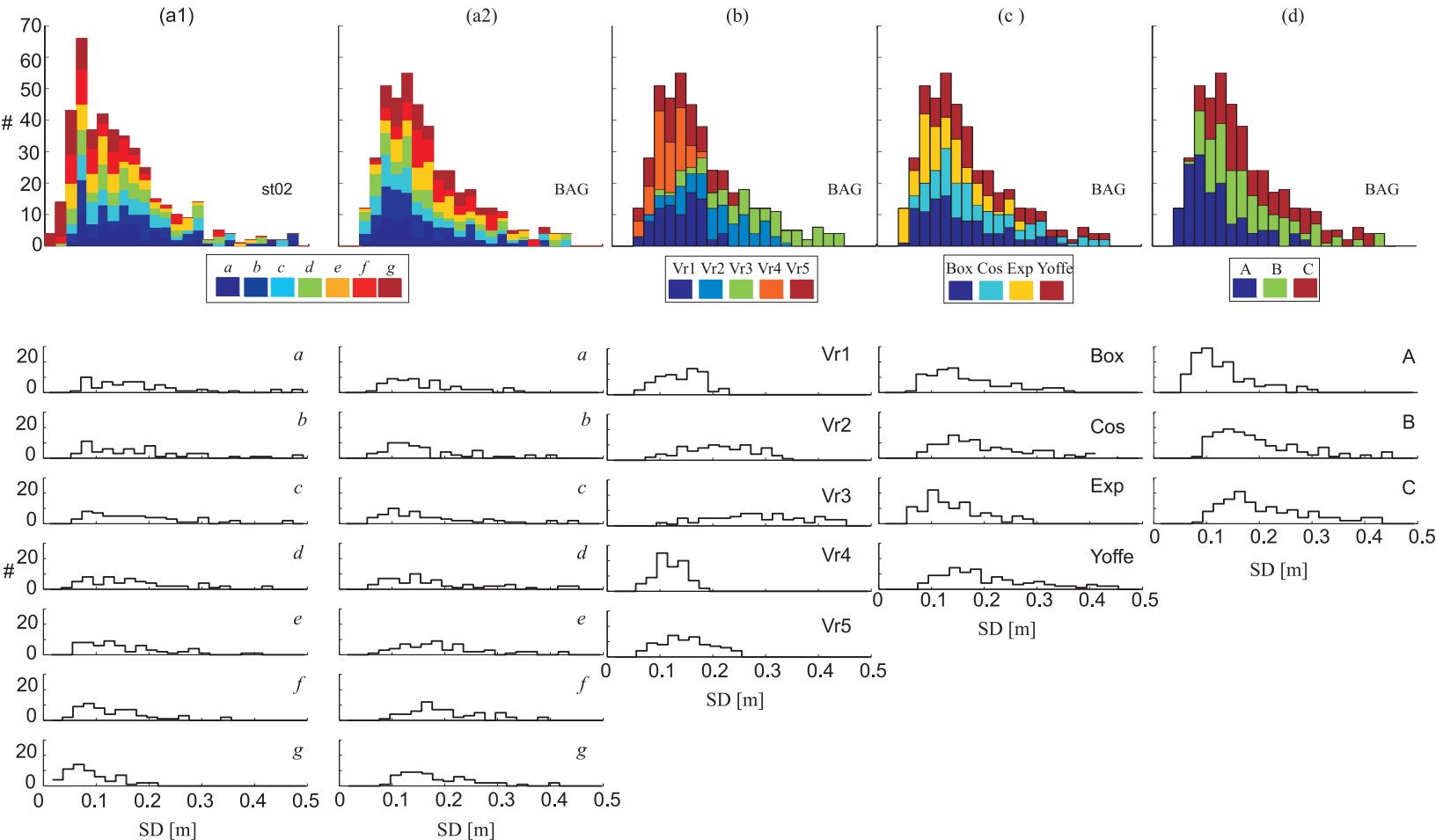
(a1)
(a2)
(b)
(c)
(d)
#
st02
BAG
a b c d e f g
Vr1 Vr2 Vr3 Vr4 Vr5
Box Cos Exp Yoffe
A B C
SD [m]

Figure 8

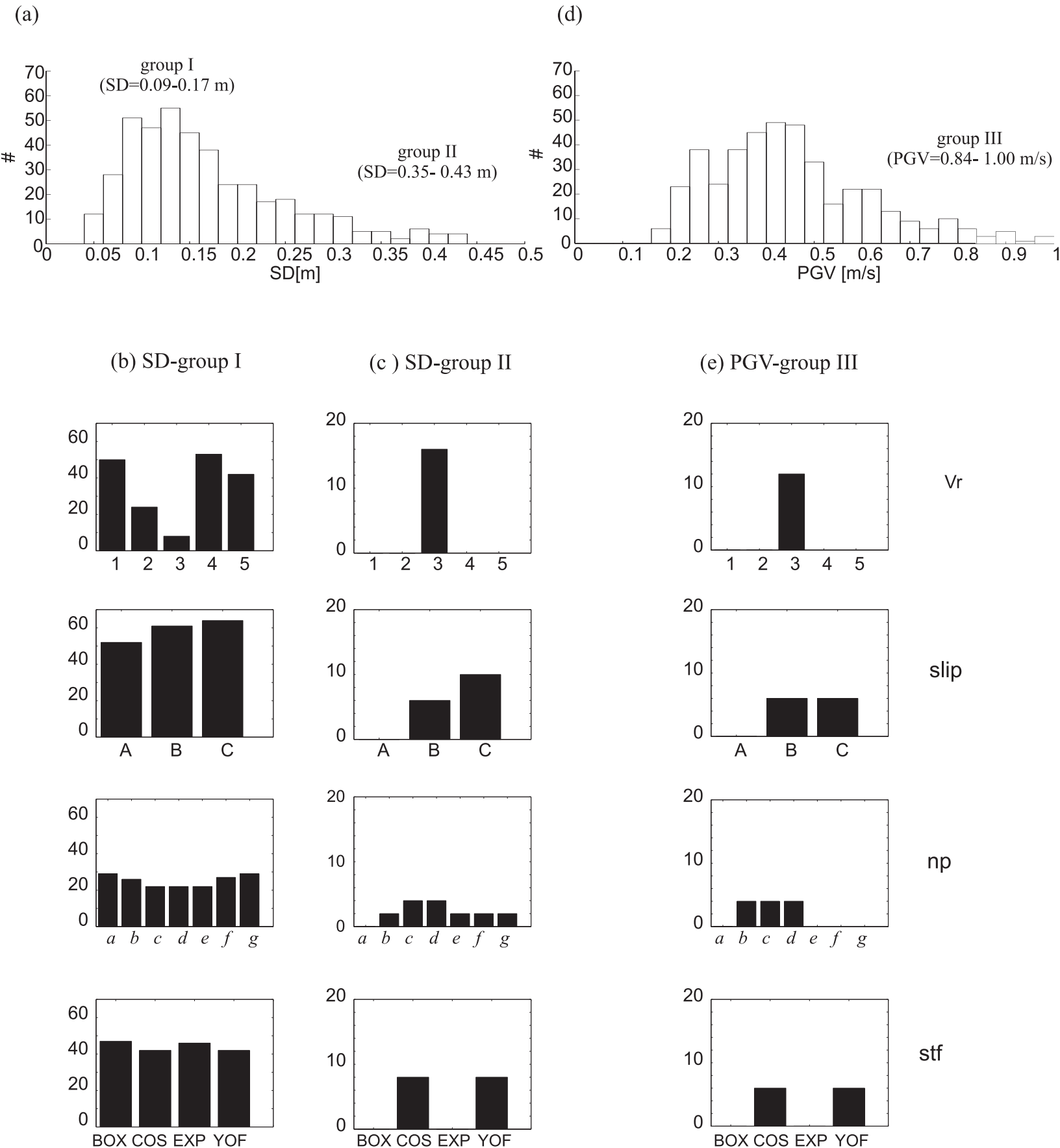
(a)
group I
(SD=0.09-0.17 m)
group II
(SD=0.35- 0.43 m)
#
SD[m]
(d)
group III
(PGV=0.84- 1.00 m/s)
PGV [m/s]
(b) SD-group I
(c) SD-group II
(e) PGV-group III
Vr
slip
np
stf
A B C
a b c d e f g
BOX COS EXP YOF

Figure 9